Stochastic electrochemical measurement of biofouling layer on gold

Sina S. Jamali *, Samuel V. Somerville, Justin J. Gooding *

School of Chemistry, Australian Centre for NanoMedicine, University of New South Wales, Sydney, 2052 Australia

Abstract

Adsorption of a biofouling layer on the surface of biosensors decreases the electrochemical activity and hence shortens the service life of biosensors, particularly implantable and wearable biosensors. Real time quantification of the loss of activity is important for *in situ* assessment of performance while presenting an opportunity to compensate for the loss of activity and recalibrate the sensor to extend the service life. Here we introduce an electrochemical noise measurement technique as a tool for quantification of the formation of a biofouling layer on the surface of gold. The technique uniquely affords thermodynamic and kinetic information without applying an external bias (potential and/or current) hence allowing the system to be appraised in its innate state. The technique relies on the analysis of non-Faradaic current and potential fluctuations that are intrinsically generated by the interaction of charged species at the electrode surface, i.e. gold. An analytical model is extended to explain the significance of parameters drawn from the statistical analysis of the noise signal. This concept is then examined in buffered media in the presence of albumin, a common protein in blood and a known source of fouling layer in biological systems. Results indicate that the statistical analysis of the noise signal can quantify the loss of electrochemical activity which is also corroborated by impedance spectroscopy as complementary technique.

Introduction

Despite tremendous scientific advances in the past few decades in making electrochemical biosensors with high specificity and sensitivity for point-of-care, wearable and implantable applications, the technology is still hampered by the issue of biofouling [1]. Non-specific adsorption of proteins and cells at the sensing electrode surface, frequently found in serum, urine, blood/plasma, and saliva, limits the access of analyte to the electrode and decreases the reactivity and response for diffusion-limited processes [2]. This rapidly decreases the signal to noise ratio and diminishes both the electrochemical signal magnitude and specificity of biosensors. The partial blockage and loss of activity, underpinned by a drop in electron transfer efficiency, halves after 3 min exposure to only 2 mg/mL albumin [3].

The majority of the effort into mitigating the impact of biofouling has gone into designing more advanced and effective anti-biofouling surface treatments, i.e. surface patterns and chemistries [2,4]. Real-time quantification of the loss of activity due to the biofouling film enables a better understanding of the *in situ* adsorption phenomena and the effectiveness of anti-biofouling strategy. It may also present an opportunity for a mathematical correction of the electrode reading by compensating for the partial blockage due to a biofouling film. The standard laboratory techniques for detection and quantification of biofouling layer including popular optical methods such as fluorescence correlation spectroscopy, ellipsometry and surface plasmon resonance, are not applicable to *in situ* measurements and point-of-care testing. The biofouling layer is often quantified electrochemically as a percentage drop in detection peak in a controlled solution with known

concentration of the analyte [5,6]. An alternative approach is the use of impedance spectroscopy that breaks down the layers and electrochemical elements of the electrode and provides quantitative measures of the biofouling layer. These techniques are useful for measurements in a controlled laboratory environment, but they are exceedingly difficult to automate and incorporate into feedback loop systems.

Stochastic electrochemical detection has come of age as a measurement method in electrophysiology, single entity electrochemistry in confined spaces [7–11] and corrosion science [12–15]. Most electrochemical processes are stochastic and discrete in nature. Yet experimental observables are typically smooth and deterministic, because of many electrochemical events or processes being averaged together. However, when the number of entities that are measured approaches a few or even one, stochasticity frequently emerges [7,16–18]. This is the basis of electrochemical stochastic measurement in nanopore [19,20] and nanofluidic [17] devices. In corrosion science, stochastic measurements capture either the average amplitude/frequency of redox events or discrete transients signifying localized reactions[21]. The current noise is typically measured between two nominally identical working electrodes coupled with a "noise-free" reference electrode that allows measurement of potential noise [22].

Inside the electrochemical cell, the noise arises from stochastic electron transfer events (oxidation and reduction), adsorption and desorption of charged species on the electrode surface[9], and the intrinsic instability of reference electrodes at micro-volt level[23,24]. The experimental data may also be tainted by environmental noise and instrumental noise[14,17,25]. The use of electrochemical noise as a quantitative measure in chemistry has predominantly been limited to the faradaic current. Very few studies have explored the non-faradaic electrochemical noise, and of those the majority are theoretical [26,27]. In this study, we measure the intrinsic thermal equilibrium noise at the electrode-electrolyte interface between a gold electrode and phosphate buffered saline (PBS). The thermal equilibrium noise is then stochasticity driven by the thermodynamic energy fluctuations of a system at thermal equilibrium (i.e. constant temperature) with no charge transfer process present at the interface (i.e. non-Faradaic current). The concept is schematically presented in Figure 1. We then developed an analytical model to explain the physical significance of quantitative outputs from measurement of non-Faradaic current and potential fluctuations. It is well-acknowledged that averaged properties, such as impedance obtained from electrochemical noise measurement, are comparable to impedance acquired from linear polarization resistance or electrochemical impedance spectroscopy [28]. We use impedance spectroscopy in this study as a complementary technique for validation of measurements. The noise measurement is then used to track the formation of a biofouling layer on gold in PBS.

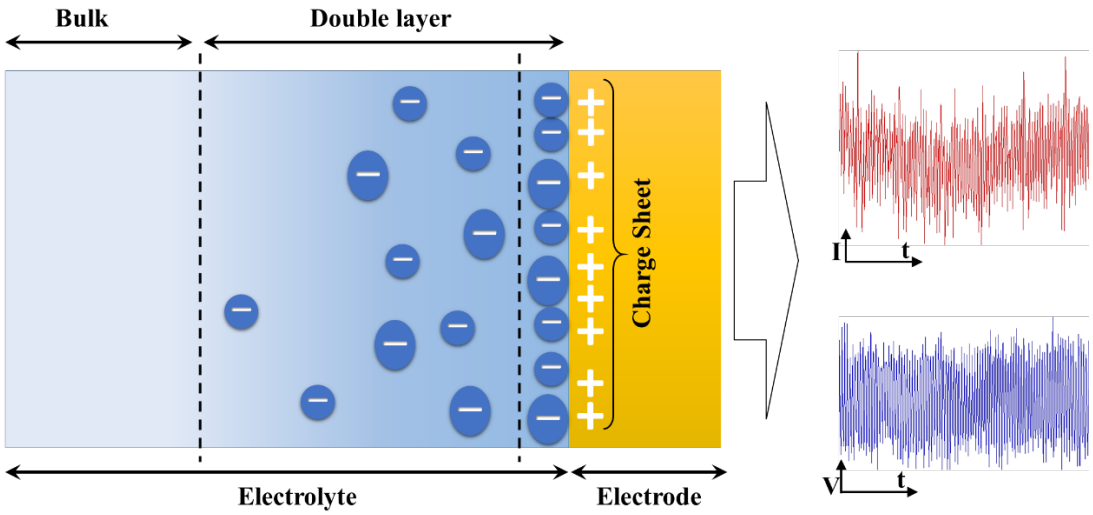

Figure 1 Schematic representation of absorbed ions on a metal electrode surface obeying the Gouy–Chapman–Stern model of the electrical double layer. In a stationary state without mass transport, the ion-electrode interaction generates thermal equilibrium noise which is measured and analysed to quantify electroactivity.

Analytical model for the current and potential fluctuation

An analytical model of the electrochemical noise at an electrode as depicted in figure 1 was derived based on the non-Faradaic (capacitive) charge transfer at the electrodes surface. When current passes through the electrode, charge is supplied by capacitance. Variation of capacitance is due to the rearrangement of ions in the electrical double layer over the active regions of the electrode surface. Therefore, the amount of capacitance and charge that passes through an electrode is also a function of its area. Partial blocking of an electrode surface reduces its active electrode area and its capacitance [29].

We employ the equivalent circuit approach introduced by the Huet group [13,30–32], where the electrochemical elements have distinct physical significance. The analytical model is derived based on the electrical equivalent circuit presented in Figure 2. This electrical equivalent circuit model differs from previous models for electrochemical noise process attenuated by an organic coating layer [33] from two main perspectives. First is that the present model considers the biofouling layer in parallel with the metal-electrolyte impedance due to the physics of the system, i.e., adsorption of the biofouling layer directly on the gold surface and the loss of activity as a result. The second difference is the electrode configuration and the sequence of measuring potential and current noise. Typically the current and potential noise are measured concurrently whereas in the approach herein the current noise is measured first followed by the measurement of potential noise. The purpose of the analytical model is to explain the physical significance of parameters extracted from the statistical analysis of electrochemical noise. The noise impedance that is regarded here as the most relevant parameter to the fouling of surface is explained mathematically, allowing it to be compared to and verified by the impedance parameter from the electrochemical impedance spectroscopy (EIS).

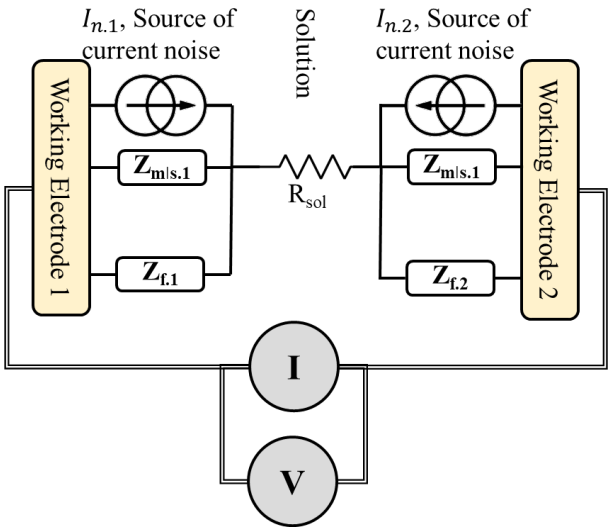

Figure 2 Electrical equivalent circuit model with current noise as the driving force in a two-electrode configuration. Z_{m-s} is interfacial impedance at metal surface and Z_f is the impedance of the biofouling film.

The electrical equivalent circuit model presented here considers current noise as the driving force in the system. The current noise source is in parallel with the respective impedance $Z_{m\text{-}s}$, otherwise known as Norton equivalent [34], as illustrated in Figure 2. The potential noise is a consequence of current noise acting on the impedance of the metal-solution interface. Discrete events that generate the current noise are considered independent from each other and also independent from the biofouling layer and the opposite working electrode, i.e. Poisson elementary noise source. Therefore, the current noise generated by each event is added to make up the current noise power of the working electrode. The term *power* is used herein (as commonly used in signal processing) to describe both the square of current and voltage, on the basis that the power dissipates in a resistive load is given by V^2/R or $I^2 \times R$.

In a typical electrochemical noise measurement, the reference electrode is considered noise-free, hence the measured potential noise is produced solely by the two working electrodes. This assumption is valid as long as the reference electrode is generating significantly lower levels of potential noise compared to working electrodes. This is frequently the case [23]. However, here the levels of potential noise generated are far lower than that typically generated by saturated Calomel or Ag|AgCl electrodes. Thus, we use the two working electrodes consecutively for the measurement of current and then potential noise to eliminate the need for a standard reference electrode. Therefore, the potential noise power from the second working electrode is added to the total measured potential noise[13]. The current noise is calculated similar to the three-electrode configuration with two noisy working electrodes and a standard "noise-less" reference electrode [35]. When the electrochemical system is in a stationary state, assumed valid only for the short duration of measurement, mass transport is assumed to have no effect on the noise as the discrete events will not create concentration gradients. The exposed surface area of the electrodes will be constant in the absence of adsorption/desorption of gas molecules. The positive and negative charge transfer reactions are assumed to be independent of each other. This is a reasonable assumption considering that the short-term pulses of negative and positive charge can be accommodated by charging and discharging of the double layer capacitance, whilst the overall charge neutrality of the electrode is maintained.

Another critical assumption in the model is that the system is electrochemically stable and stationary for the duration of the measurement, thus the statistical analyses of current and potential noise are related. This allows calculation of the noise resistance, R_n, as the ratio σ_V/σ_I (standard deviation of potential noise/standard deviation of current noise)[36]. This would not be true in a system with distinct current and potential transients as these events will not be "mirrored" from the current pulses to the potential pulses. However, in a stationary system without localised electrochemical events, such as the system examined herein, the current and potential signals are considered to carry similar signatures and be able to be solved mathematically together.

The measured current noise of one working electrode is produced by the flow of current from one electrode to the other. For identical electrodes, i.e. $Z_{m\text{-}s1} = Z_{m\text{-}s2}$, in the absence of surface layer and solution resistance, the current generated by WE1 will be halved, with one half flowing towards WE2 and the other half dissipating in ionic collision events [37]. Only the current that flows towards the second working electrode is detectable by ammeter and is measured as current noise power. Therefore, the current noise power of each of the identical electrodes will be given by equation 1,

$$\overline{I_{n\,measured}^2} = \frac{\overline{I_n^2}}{4} \qquad (1)$$

Where $I_{n\,measured}$ is current noise recorded by the ammeter and $\overline{I_n{}^2}$ is the mean square noise current or current noise power. Assuming the currents from the two electrodes are uncorrelated, the current noise power resulting from the two identical electrodes is the sum of current noise power produced by each electrode and is given by equation 2,

$$\overline{I^2_{n\,measured}} = \frac{\overline{I_n{}^2}}{2} \qquad (2)$$

In the presence of solution resistance, the proportion of current from one electrode to the other will be reduced due to the additional solution resistance in the circuit. Therefore the measured current noise power is decreased proportional to $\frac{Z_{m-s}}{Z_{m-s1}+Z_{m-s2}+R_S}$ and is given by equation 3 [38],

$$\overline{I^2_{n\,measured}} = \left(\frac{Z_{m-s.1}}{R_S+Z_{m-s.1}+Z_{m-s.2}}\right)^2 . \overline{I_{n2}{}^2} + \left(\frac{Z_{m-s.2}}{R_S+Z_{m-s.1}+Z_{m-s.2}}\right)^2 . \overline{I_{n1}{}^2}$$

$$\overline{I^2_{n\,measured}} = \left(\frac{Z_{m-s.1}\,.\,I_{n2} + Z_{m-s.2}\,.\,I_{n1}}{R_S+Z_{m-s.1}+Z_{m-s.2}}\right)^2 \qquad (3)$$

where $Z_{m-s.1}$ and $Z_{m-s.2}$ are metal-solution impedances of WE1 and WE2 respectively. Equation 4 can be simplified for the case of symmetric (identical) electrodes in the form of equation 4. Herein three possible sources of electrode asymmetry, i.e., non-identical metal-solution impedance, film impedance and solution resistance, have been assumed symmetrical to simplify equation 4.

$$\overline{I^2_{n\,measured}} = 2\left(\frac{Z_{m-s}}{R_S+2Z_{m-s}}\right)^2 . \overline{I_n{}^2} \qquad (4)$$

Assuming $Z_f \gg Z_{m-s}$, the current does not flow through the biofouling film (in parallel with the Z_{m-s}) and therefore is unaffected.

The potential noise power in the absence of solution resistance and surface layer is produced by the current acting on the interfacial impedance ($Z_{m\text{-}s}$) at the surface of the electrode that generates the current, in parallel with the solution resistance and polarisation resistance of the second electrode. The potential noise power for one source of current, i.e. one working electrode, is given by equation 5 [38],

$$\overline{E_n{}^2} = \frac{\overline{I_n{}^2}\ Z_{m-s}{}^2}{4} \qquad (5)$$

Where $\overline{E_n{}^2}$ is mean square potential noise or potential noise power, $\overline{I_n{}^2}$ is mean square current noise or current noise power, and Z_{m-s} is interfacial impedance at metal surface. In order to calculate the potential noise power in the presence of solution resistance and film impedances the effects of each source of current should be analysed independently, with all other voltage sources treated as short-circuit and current sources as open-circuit. Considering the current noise source $I_{n.1}$ on WE1, the current $I_{n.1}$ will be split between the $Z_{m\text{-}s.1}$ and the R_{sol}+ $Z_{m\text{-}s.2}$. Note that assuming $Z_f \gg Z_{m-s}$, current does not flow through $Z_{f.1}$ and $Z_{f.2}$ thus the impedance of the biofouling film does not generate potential noise. Using || to indicate parallel impedances and + to indicate series impedances, $I_{n.1}$ will be applied to an impedance $Z_{m\text{-}s.1} \parallel (R_{sol}+Z_{m\text{-}s.2})$, hence producing a voltage $E_1 = I_{n1} \times (Z_{m\text{-}s.1} \parallel (R_{sol}+Z_{m\text{-}s.2}))$. The potential will be measured between the two electrodes and therefore the proportion of I_{n1} that generated potential noise on WE1 and WE2 should be considered separately and added to obtain the total potential noise as a result of I_{n1}.

Using the current divider rule, the current flowing through the chain impedance of R_{sol}+$Z_{m\text{-}s.2}$ will be equal to

$$I_{n.1} = I_n \times \frac{Z_{m-s1}}{Z_{m-s1}+R_s+Z_{m-s2}} \quad (6)$$

Similarly, the current flowing through the $Z_{m\text{-}s.1}$ will be given by

$$I_{n.1} = I_n \times \frac{R_s+Z_{m-s2}}{Z_{m-s1}+R_s+Z_{m-s2}}$$

Replacing this current in the ohmic relationship for the potential noise generated by $I_{n.1}$ flowing through $Z_{m\text{-}s.1}$ and $Z_{m\text{-}s.2}$ will give equation 8 representing the potential noise as a result of WE1 in an asymmetrical configuration.

$$E_{n.1} = I_{n.1} \times \frac{Z_{m-s.1}}{Z_{m-s1}+R_s+Z_{m-s2}} \times Z_{m-s.2} + I_{n.1} \times \frac{Z_{m-s.2}+R_s}{Z_{m-s1}+R_s+Z_{m-s2}} \times Z_{m-s.1} \quad (7)$$

For a symmetrical configuration, i.e. $Z_{m\text{-}s} = Z_{m\text{-}s.1} = Z_{m\text{-}s.2}$, equation 7 simplifies to,

$$E_{n.1} = I_{n.1} \times Z_{m-s} \quad (8)$$

Therefore, the potential noise power as a result of the two identical working electrodes is calculated by replacing I_n from equation 2 and is given by equation 9.

$$\overline{E^2_{n\,measured}} = \frac{\overline{I_n^2} \times {Z_{m-s}}^2}{2} \quad (9)$$

The noise resistance is defined as the ratio of the standard deviations of the potential and current noise or $R_n = \sqrt{\overline{E_n^2}/\overline{{I_n}^2}}$. Replacing $\overline{{I_n}^2}$ and $\overline{E_n^2}$ from equations 4 and 9 yields equation 10.

$$R_n = \frac{R_s}{2} + Z_{m-s} \quad (10)$$

For negligible solution resistance, the equation 10 simplifies to $R_n = Z_{m-s}$. The impact of the biofouling layer and change in the active surface area of the electrodes comes into effect by considering the effect of surface area on I_n and Z_{m-s} separately. The power of current noise, when considered to be generated by independent and uncorrelated current sources, from various regions of the electrode surface will add up. Therefore the variance of the current noise is proportional to the area, and the amplitude of the current noise (measured as the standard deviation) is proportional to $\sqrt{area}$ [13,39,40]. The amplitude of the potential noise, being the result of application of current noise to $Z_{m\text{-}s}$, will decrease by increasing the area proportional to $1/\sqrt{area}$. Based on this analysis, the noise resistance has a linear relationship with $1/area$. Note that this relationship will change in the case of correlated current noise sources.

Experimental Methods

Dulbecco's phosphate-buffered saline (DPBS) from ThermoFisher was used as media and contained $CaCl_2$ (100 mg/L), $MgCl_2$-6H2O (100 mg/L), KCl (200 mg/L), KH_2PO_4 (200 mg/L), NaCl (8 g/L), Na_2HPO_4-7H_2O (2.16 g/L). Bovine serum albumin (≥98%, ~66 kDa) from Sigma-Aldrich was used as the fouling agent and dissolved in DPBS at 4 g/dL.

Electrochemical noise data acquisition was performed using a combination of a signal (potential or current) amplifier, a data acquisition module and a computer program for data logging and primary analysis. SR560 Voltage Preamplifier and SR570 Current Preamplifier from Stanford Research Systems were used for pre-amplification of noise data prior to analog to digital conversion. These instruments

enable a low noise amplification of the signal with negligible input noise (i.e., 4 nV/√Hz input noise and 5 fA/√Hz input noise, respectively) and low (<1 mV) potential burden. They also provide selectable analog filters setting that have been used in this study to eliminate out-of-range noise power added to the measured signal. NI-9239 (National Instruments) with differential analog input was used as data acquisition providing a 24-bit analog to digital conversion with nominal input noise of 70 µV. The module enables high-speed data acquisition of up to 50,000 samples per second. The computer program SIGVIEW v6.0 was used for data logging and signal processing. The principle of selecting sampling frequency, signal conditioning (using filters) and post-treatment of data is given in supporting information. Gold disk electrodes, 2 mm in diameter (PalmSens BV), were used as working electrodes, WE1 and WE2, in the electrochemical noise measurement experiments.

EIS was performed using PalmSens 4 in frequency scan mode within 100 kHz - 0.01 Hz range with 10 mV root mean square around open circuit potential. In EIS experiments gold disk electrodes were used as the working electrode, WE, Pt mesh as the counter electrode and a leakless Ag|AgCl (3.4 M KCl) , supplied by eDAQ, used as reference electrodes. Figure S1 in supporting information schematically shows the electrode configuration used for the electrochemical noise measurement and EIS experiments.

WEs were polished using alumina powder, successively reducing particle size from 1 µm to 0.03 µm, rinsed with acetone and then electrochemically cleaned in H_2SO_4 (0.5 M) until a stable cyclic voltammogram was observed. A representative cyclic voltammetry plot from the electrochemical cleaning of Au disk electrodes is provided in the Supporting Information Figure S2.

Results and discussion

Instrument noise was measured to attain a baseline above which meaningful electrochemical noise data can be acquired. The instrument noise is measured using electronic resistors with resistances in the range of those expected from the electrochemical cell. Figure 3 shows spectral power density of potential and current for instrumental noise measured via 100 kΩ (Figures 3a and 3b) and 10 MΩ (Figures 3c and 3d). The theoretical value of the thermal noise generated by the associated resistors was also calculated and shown as a broken baseline in each plot. Thermal noise of a resistor with resistance R (in Ohms) is calculated as 6 kTR for the potential thermal noise and 2 kT/R for the current (Boltzmann's constant $k=1.38\times10^{-23}$ J/K and T=293 °K). Potential and current noise raw data in time domain are provide in Supporting Information Figure S3. Both the potential and current noise exhibit Poisson distribution with no systematic noise due to the circuitry/instrument.

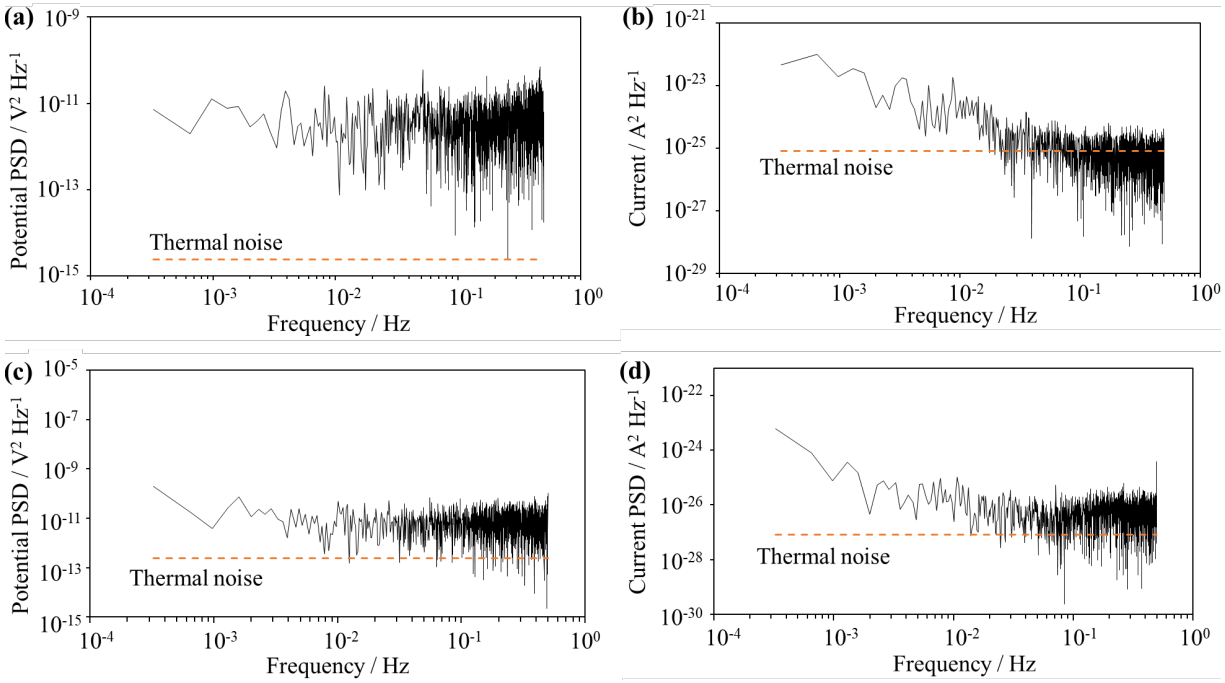

Figure 3 Instrument noise measured using fixed value resistors of (a & b) 100 kΩ and (c & d) 10 MΩ, presented as power spectral density in frequency domain for potential and current noise.

The background noise is measured for two Au working electrodes in PBS solution. Figure 4 presents electrochemical noise in the time domain (Figure 4a) and frequency domain (Figure 4b) as well as spectral noise impedance (R_{sn}) plotted with AC impedance (Z) in Figure 4c. A representative Nyquist and Bodé plot for the gold electrode in PBS is provided in Supporting Information Figure S4. The noise resistance directly from statistical analysis of the time domain data is calculated as $R_n = \sigma_V/\sigma_I$ and shown as an asterisk in Figure 4c. Comparison between Figure 4a & 4b and the levels of instrument noise (Figure 3) confirms that the background noise from the electrochemical system is significantly higher than the instrumental noise at all frequencies. The average current noise power from the instrumentation with a 10 MΩ resistor is in the order of 10^{-26} A^2 whereas the current noise from the electrochemical cell is in the order 10^{-22} A^2. This means that the contribution of instrument noise in the measured signal is insignificant. Similarly, the potential noise power from the 10 MΩ resistor averages around the order of 10^{-11} V^2 whereas the electrochemical system generates potential noise power in the order of 10^{-10} V^2 and higher. The spectral noise impedance decreases slightly at higher frequencies due to the internal low-pass filters. Both the R_n and R_{sn} measured values are slightly higher than the AC impedance. In the absence of a net current flowing through the interface, which corresponds to no charge transfer process at the interface i.e., non-faradaic electrodes, only thermal noise is anticipated. Hence, the spectral density of the measured noise relies on the macroscopic equivalent circuit model of the experimental setup, and its possible frequency dependencies [27]. This is distinctively different from the non-equilibrium excess noise caused by charge transfer kinetics and relaxation currents produced by mass transfer processes, which would exhibit $1/f$ and $1/f^2$ dependency in the power spectral density.

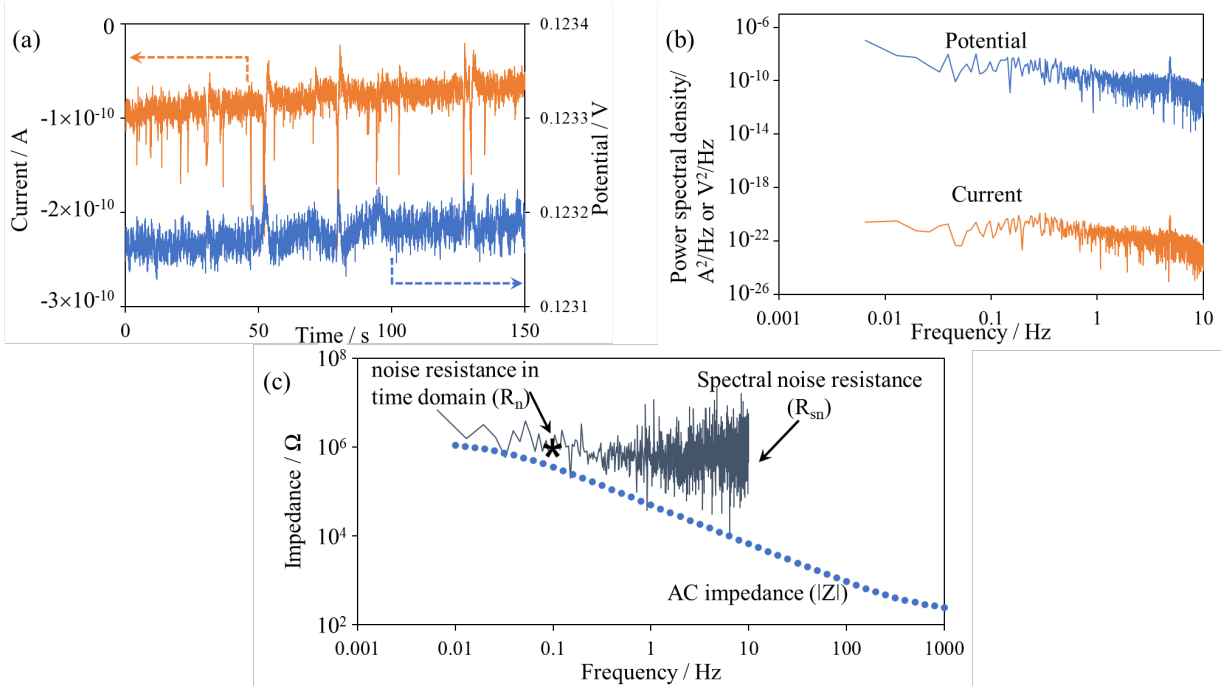

Figure 4 Background noise and impedance measured from the Au disc electrodes (d=2 mm) in PBS. a) is the current and potential in time domain data, b) is the power spectral density in the frequency domain, and c) is the overlay of spectral noise impedance (R_{sn}), AC impedance (Z) and the noise resistance from time domain analysis (R_n).

The thermal equilibrium noise (i.e. Johnson-Nyquist noise) originates from the adsorption and interaction of chloride with the gold surface. It has been shown that at potentials higher than the potential of zero charge, anions such as chloride predominantly absorb and interact with conductive surfaces such as gold in aqueous media establishing an electrical double layer [41,42]. The potential of zero charge was calculated for the gold electrode in PBS using the principle of minimum differential capacitance [43,44]. This is explained in more detail in the supporting information. The EIS data, with potential sweep and the calculated values of differential capacitance versus potential, are provided in supporting information Figures S5 and S6. The variation of open circuit potential value of the gold electrode in PBS and PBS with 4 g/dL BSA added are provided in supporting information Figure S7. Analysis is performed to elucidate the source of electrochemical noise rather than an in-depth analysis of surface charge and its variation with the formation of biofilm. Data confirms that the gold electrode in both electrolytes establishes an open circuit potential well-above the potential of zero charge indicating an absorbed layer of anions on the gold as depicted in Figure 1.

The formation of biofouling layer was observed as the evolution of noise resistance over the time of exposure to 4 g/dL BSA in PBS solution. The result presented in Figure 5a shows spectral noise impedance after 10 min, 2.5 h and 24 h in the solution. The R_{sn} increases at all frequencies from 10 min immersion to 2.5 h and then 24 h immersion. The evolution of R_n values (calculated from time domain analysis) are plotted in Figure 5b showing a sharp increase in the first 2.5 h of immersion followed by a plateau. It is noteworthy that while the stationary state of the system was an assumption in derivation of the theoretical model, this assumption is not strictly true in practice. The formation of biofouling film alters both the thermodynamic and kinetic of the system. One approach to reducing the effect of non-stationary behavior is to use a sequence of short time records, so that the signal is close to being stationary over the period analysed. This also has the advantage of revealing the

changes in behavior with time and is the basis of the short-time Fourier transform [45]. As noted above, this is subject to the uncertainty principle, so there is a trade-off between resolution in time (which requires a short segment of time record), and resolution in frequency (which requires a long segment)[46]. With the system at thermodynamic equilibrium, i.e. zero bias, the power spectral density of the current noise and of the voltage noise are expected to follow the apparent electrochemical impedance as implied by equation 10 [47].

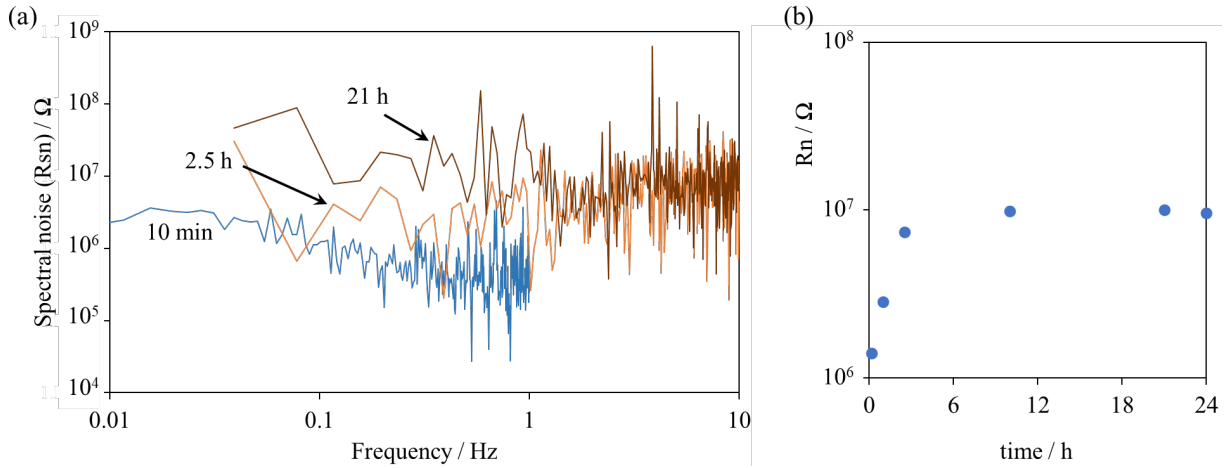

Figure 5 Noise characteristics of gold electrode in PBS + 4 g/dL BSA over time represented by (a) the spectral noise resistance (R_{sn}) in frequency domain after 10 min, 2.5 h and 24 h immersion and (b) the continuous evolution of noise resistance (R_n) from time domain analysis over 24 h immersion.

Figure 6a shows evolution of the AC impedance (Z) in PBS + 4 g/dL BSA after 10 min, 1 h, 2 h, 3 h, 6 h, 10 h and 24 h immersion. A Randles circuit (given in Supporting Information Figure S8) is fitted as the equivalent electrical circuit comprising the solution resistance in series with a parallel resistor (R_{ct}) and constant phase element, consistent with previous studies[48]. The R_{ct} represents the electrode/electrolyte interface and is considered analogous to the $Z_{m-s} + Z_f$ or the polarization resistance in Figure 2. The exponent (n) term for the constant phase element is indicative of deviation from the ideal capacitor behaviour. The values of R_{ct} are calculated by electrical equivalent circuit model fitting and plotted against the immersion time in Figure 6b showing an initial increase in the charge transfer resistance followed by a plateau, similar to the trend observed in Figure 5b. The corresponding Nyquist and Bode plots are provided in supporting information Figure S9. Following exposure to BSA, the impedance at low frequencies increased compared to the uncoated electrode. There were shifts in the phase angle with longer immersion time indicating a more capacitive behavior at high frequencies and more resistive at intermediate frequencies. In general, the charge transfer resistance increased, and admittance decreased, consistent with the increasing total impedance trend at low frequencies. These trends are all indicative of a decrease in effective electrode area, which increases low frequency impedance and polarization resistance and decreases admittance. The impedance (Z) plateaus approximately after 3 h is consistent with the frequently reported behaviour of the surface blocking properties of BSA [6,48–50]. BSA is a globular protein (14 × 4 nm) in blood plasma with a molecular weight of~66 KDa and known to readily adsorb on gold resulting in an increase of double layer capacitance and increase in the charge transfer resistance [48].

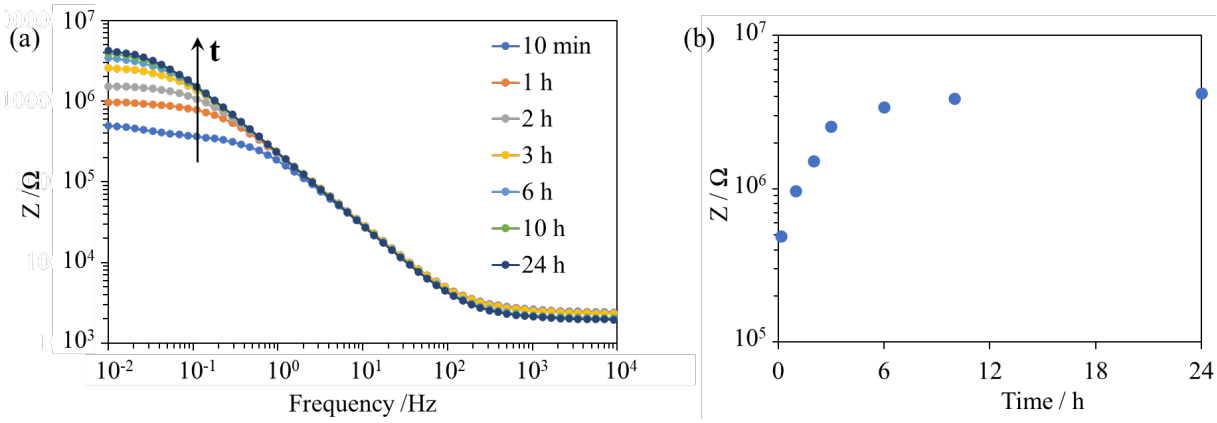

Figure 6 Evolution of (a) Bodé plots, and (c) R_{ct} values for a gold electrode (d=2 mm) over 24 h immersion in PBS + 4 g/dL BSA due to formation of BSA layer on the surface. The Bodé plots are provided at immersion times of 10 min, 1 h, 2 h, 3 h, 6 h, 10 h and 24 h. The R_{ct} values were calculated by electrical equivalent circuit fitting on EIS data. The Nyquist and Bodé plots (including Bode phase plots) are provided in supporting information Figure S9.

Figure 7 provides a comparison point for the values of AC impedance (Z), R_n and R_{sn} for the gold electrode after 24 h in PBS with 4 g/dL BSA added. The R_n is a close approximation of R_{sn} over the range of analysed frequency and is in good agreement with the Z at low frequency (i.e. DC limit). It is important to note that Z is a frequency dependent parameter whereas the R_{sn}, which has originated from thermal equilibrium noise is fundamentally frequency independent. It is also noteworthy that discrepancy between the noise resistance and AC impedance may arise due to lack of conditions that were assumed to be true for the analytical modelling of noise signal. For example, in the electrical equivalent circuit model, the current was assumed to flow only through the $Z_{m\text{-}s}$ element and not the Z_f due to the assumption of $Z_f \gg Z_{m\text{-}s}$. Similarly, the potential noise was assumed to be unaffected by Z_f. However, in practice the adsorbed layer of protein does not completely passivate the gold surface and also the electrical double layer at the interface of BSA/gold does play a part in compensating charge imbalance that is caused by the current noise. In practice, the noise resistance appears to provide a close approximation of polarization resistance and holds promise for real time measurement of loss of surface activity due to fouling of electrode.

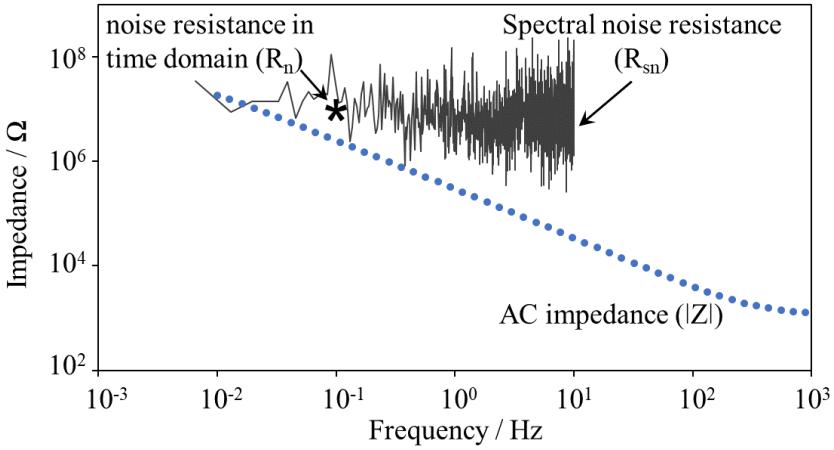

Figure 7 A comparison between the impedance values of a gold electrode (d=2 mm) after 24 h immersion in PBS + 4 g/dL BSA obtained by EIS and electrochemical noise technique. The AC

impedance (Z) and spectral noise impedance (R_{sn}) are lotted against the frequency component and the R_n from time domain analysis of the noise data is shown as a point value at 0.1 Hz (the sampling frequency).

Conclusion

The present work lays the foundation for stochastic electrochemical measurement of impedance from thermal equilibrium noise data. The thermal equilibrium noise manifested as non-Faradaic current and potential fluctuation from the absorbed ions on the surface of an electrode is theoretically modelled using equivalent electrical circuit and then examined experimentally. The technique is showcased here as a tool to quantify loss of activity due to biofouling of a gold electrode.

The analytical model shows the significance and relevance of parameters that are extracted from statistical analysis of noise signal. In particular, the noise resistance is shown to be theoretically analogous to the polarization resistance. The thermal equilibrium noise can be experimentally measured with a sensitive instrument and the variation in the noise resistance is shown both mathematically and experimentally to reflect changes in active surface area due to formation of a fouling layer. Noise resistance analysis is corroborated by electrochemical impedance spectroscopy.

A particular appeal of the electrochemical noise measurement technique for the point-of-care, wearable and implantable biosensor applications is the absence of the reference electrode. Reference electrodes in biosensing systems are typically in a quasi-stationary state with electrochemical properties that can be altered depending on the electroactive species and biofouling of the electrode. Any change in the stationary state of the pseudo-reference electrode adds to the ambiguity of the measured values. Another unique advantage of electrochemical noise measurement is the possibility of acquiring information without application of external bias (voltage and/or current), hence examining surface phenomena in their most innate state. We envision that the technique holds promise for real time approximation of biofouling and loss of activity in sensors and eventually could be used to compensate for the signal loss due to biofouling in real time.

Acknowledgements

S.J. acknowledges ARC grant under the Discovery early career research award (DECRA) scheme, Grant No. DE210101137.

References

(1) Barfidokht, A.; Gooding, J. J. Approaches Toward Allowing Electroanalytical Devices to Be Used in Biological Fluids. *Electroanalysis* **2014**, *26* (6), 1182–1196. https://doi.org/10.1002/elan.201400097.

(2) Russo, M. J.; Han, M.; Desroches, P. E.; Manasa, C. S.; Dennaoui, J.; Quigley, A. F.; Kapsa, R. M. I.; Moulton, S. E.; Guijt, R. M.; Greene, G. W.; Silva, S. M. Antifouling Strategies for Electrochemical Biosensing: Mechanisms and Performance toward Point of Care Based Diagnostic Applications. *ACS Sensors* **2021**, *6* (4), 1482–1507. https://doi.org/10.1021/acssensors.1c00390.

(3) Patel, J.; Radhakrishnan, L.; Zhao, B.; Uppalapati, B.; Daniels, R. C.; Ward, K. R.; Collinson, M. M. Electrochemical Properties of Nanostructured Porous Gold Electrodes in Biofouling

Solutions. *Anal. Chem.* **2013**, *85* (23), 11610–11618. https://doi.org/10.1021/ac403013r.

(4) Lin, P. H.; Li, B. R. Antifouling Strategies in Advanced Electrochemical Sensors and Biosensors. *Analyst* **2020**, *145* (4), 1110–1120. https://doi.org/10.1039/c9an02017a.

(5) Moulton, S. .; Barisci, J. .; Bath, A.; Stella, R.; Wallace, G. . Studies of Double Layer Capacitance and Electron Transfer at a Gold Electrode Exposed to Protein Solutions. *Electrochim. Acta* **2004**, *49* (24), 4223–4230. https://doi.org/10.1016/j.electacta.2004.03.034.

(6) Moulton, S. E.; Barisci, J. N.; Bath, A.; Stella, R.; Wallace, G. G. Investigation of Protein Adsorption and Electrochemical Behavior at a Gold Electrode. *J. Colloid Interface Sci.* **2003**, *261* (2), 312–319. https://doi.org/10.1016/S0021-9797(03)00073-0.

(7) Ren, H.; Edwards, M. A. Stochasticity in Single-Entity Electrochemistry. *Curr. Opin. Electrochem.* **2021**, *25*, 100632. https://doi.org/10.1016/j.coelec.2020.08.014.

(8) Kätelhön, E.; Krause, K. J.; Singh, P. S.; Lemay, S. G.; Wolfrum, B. Noise Characteristics of Nanoscaled Redox-Cycling Sensors: Investigations Based on Random Walks. *J. Am. Chem. Soc.* **2013**, *135* (24), 8874–8881. https://doi.org/10.1021/ja3121313.

(9) Singh, P. S.; Chan, H.-S. M.; Kang, S.; Lemay, S. G. Stochastic Amperometric Fluctuations as a Probe for Dynamic Adsorption in Nanofluidic Electrochemical Systems. *J. Am. Chem. Soc.* **2011**, *133* (45), 18289–18295. https://doi.org/10.1021/ja2067669.

(10) Singh, P. S.; Lemay, S. G. Stochastic Processes in Electrochemistry. *Anal. Chem.* **2016**, *88* (10), 5017–5027. https://doi.org/10.1021/acs.analchem.6b00683.

(11) Lemay, S. G. Noise as Data: Nucleation of Electrochemically Generated Nanobubbles. *ACS Nano* **2019**, *13* (6), 6141–6144. https://doi.org/10.1021/acsnano.9b03348.

(12) Xia, D. H.; Deng, C. M.; Macdonald, D.; Jamali, S.; Mills, D.; Luo, J. L.; Strebl, M. G.; Amiri, M.; Jin, W.; Song, S.; Hu, W. Electrochemical Measurements Used for Assessment of Corrosion and Protection of Metallic Materials in the Field: A Critical Review. *J. Mater. Sci. Technol.* **2022**, *112*, 151–183. https://doi.org/10.1016/j.jmst.2021.11.004.

(13) Xia, D.-H.; Song, S.; Behnamian, Y.; Hu, W.; Cheng, Y. F.; Luo, J.-L.; Huet, F. Review—Electrochemical Noise Applied in Corrosion Science: Theoretical and Mathematical Models towards Quantitative Analysis. *J. Electrochem. Soc.* **2020**, *167* (8), 081507. https://doi.org/10.1149/1945-7111/ab8de3.

(14) Bosch, R.; Cottis, R. A.; Csecs, K.; Dorsch, T.; Dunbar, L.; Heyn, A.; Hyökyvirta, O.; Kerner, Z.; Kobzova, A.; Macak, J.; Novotny, R.; Öijerholm, J.; Piippo, J.; Richner, R.; Ritter, S.; Sánchez-amaya, J. M.; Somogyi, A.; Väisänen, S. Reliability of Electrochemical Noise Measurements: Results of Round-Robin Testing on Electrochemical Noise. *Electrochim. Acta* **2014**, *120*, 379–389. https://doi.org/10.1016/j.electacta.2013.12.093.

(15) Jamali, S. S.; Zhao, Y.; Gao, Z.; Hee, A. C. In Situ Evaluation of Corrosion Damage Using Non-Destructive Electrochemical Measurements – a Case Study. *J Ind Eng Chem* **2016**, *43*, 36–43. https://doi.org/10.1016/j.jiec.2016.07.045.

(16) Kätelhön, E.; Krause, K. J.; Mathwig, K.; Lemay, S. G.; Wolfrum, B. Noise Phenomena Caused by Reversible Adsorption in Nanoscale Electrochemical Devices. *ACS Nano* **2014**, *8* (5), 4924–4930. https://doi.org/10.1021/nn500941g.

(17) Zevenbergen, M. A. G.; Singh, P. S.; Goluch, E. D.; Wolfrum, B. L.; Lemay, S. G. Stochastic Sensing of Single Molecules in a Nanofluidic Electrochemical Device. *Nano Lett.* **2011**, *11* (7), 2881–2886. https://doi.org/10.1021/nl2013423.

(18) Lemay, S. G.; Kang, S.; Mathwig, K.; Singh, P. S. Single-Molecule Electrochemistry: Present Status and Outlook. *Acc. Chem. Res.* **2013**, *46* (2), 369–377.

https://doi.org/10.1021/ar300169d.

(19) Ying, Y. L.; Hu, Z. L.; Zhang, S.; Qing, Y.; Fragasso, A.; Maglia, G.; Meller, A.; Bayley, H.; Dekker, C.; Long, Y. T. Nanopore-Based Technologies beyond DNA Sequencing. *Nat. Nanotechnol.* **2022**, *17* (11), 1136–1146. https://doi.org/10.1038/s41565-022-01193-2.

(20) Wu, Y.; Gooding, J. J. The Application of Single Molecule Nanopore Sensing for Quantitative Analysis. *Chemical Society Reviews*. 2022, pp 3862–3885. https://doi.org/10.1039/d1cs00988e.

(21) Cottis, R. A.; Homborg, A. M.; Mol, J. M. C. The Relationship between Spectral and Wavelet Techniques for Noise Analysis. *Electrochim. Acta* **2016**, *202*, 277–287. https://doi.org/10.1016/j.electacta.2015.11.148.

(22) ISO/DIS 17093 Corrosion of Metals and Alloys — Guidelines for Corrosion Test by Electrochemical Noise Measurements. **2015**.

(23) Jamali, S. S.; Mills, D. An Assessment of Intrinsic Noise of Pseudo-Reference Electrodes and Instrumental Noise to Enable Reliable Electrochemical Noise Measurements in Situ on Organically Coated Metal. *Electrochim. Acta* **2021**, *398*, 139279. https://doi.org/10.1016/j.electacta.2021.139279.

(24) Bertocci, U.; Huet, F.; Nogueira, R. P. Use of Multiple Reference Electrodes in Electrochemical Noise Measurements. *Corrosion* **2003**, *59* (7), 629–634. https://doi.org/10.5006/1.3277593.

(25) Bertocci, U.; Huet, F. Noise Resistance Applied to Corrosion Measurements III. Influence of the Instrumental Noise on the Measurements. *J. Electrochem. Soc.* **1997**, *144* (8), 2786–2793. https://doi.org/10.1149/1.1837896.

(26) Hoang Ngoc Minh, T.; Kim, J.; Pireddu, G.; Chubak, I.; Nair, S.; Rotenberg, B. Electrical Noise in Electrolytes: A Theoretical Perspective. *Faraday Discuss.* **2023**. https://doi.org/10.1039/d3fd00026e.

(27) Hassibi, A.; Navid, R.; Dutton, R. W.; Lee, T. H. Comprehensive Study of Noise Processes in Electrode Electrolyte Interfaces. *J. Appl. Phys.* **2004**, *96* (2), 1074–1082. https://doi.org/10.1063/1.1755429.

(28) Jamali, S. S.; Mills, D. J. A Critical Review on Electrochemical Noise Measurement as a Tool for Evaluation of Organic Coatings. *Prog. Org. Coatings* **2016**, *95*, 13–17. https://doi.org/10.1016/j.porgcoat.2016.02.016.

(29) Harris, A. R.; Carter, P.; Cowan, R.; Wallace, G. G. Impact of Protein Fouling on the Charge Injection Capacity, Impedance, and Effective Electrode Area of Platinum Electrodes for Bionic Devices. *ChemElectroChem* **2021**, *8* (6), 1078–1090. https://doi.org/10.1002/celc.202001574.

(30) Gabrielli, C.; Huet, F.; Keddam, M. Fluctuations in Electrochemical Systems. I. General Theory on Diffusion Limited Electrochemical Reactions. *J. Chem. Phys.* **1993**, *99* (9), 7232–7239. https://doi.org/10.1063/1.465440.

(31) Aballe, a.; Huet, F. Noise Resistance Applied to Corrosion Measurements: VI. Partition of the Current Fluctuations Between the Electrodes. *J. Electrochem. Soc.* **2002**, *149* (3), B89. https://doi.org/10.1149/1.1449952.

(32) Bertocci, U.; Gabrielli, C.; Huet, F.; Keddam, M. Noise Resistance Applied to Corrosion Measurements. I. Theoretical Analysis. *J. Electrochem. Soc.* **1997**, *144* (1), 31–37.

(33) Jamali, S. S.; Mills, D. J.; Cottis, R. A.; Lan, T. Y. Analysis of Electrochemical Noise Measurement on an Organically Coated Metal. *Prog. Org. Coatings* **2015**, *96*, 52–57.

https://doi.org/10.1016/j.porgcoat.2016.01.017.

(34) Curioni, M.; Cottis, R. A.; Di Natale, M.; Thompson, G. E. Electrochemical Noise Analysis on Multiple Dissimilar Electrodes: Theoretical Analysis. *Electrochim. Acta* **2011**, *56* (27), 10270–10275. https://doi.org/10.1016/j.electacta.2011.09.013.

(35) ISO 17093: Corrosion of Metals and Alloys, Guidelines for Corrosion Test by Electrochemical Noise Measurements. 2015.

(36) Mészáros, G.; Szenes, I.; Lengyel, B. Measurement of Charge Transfer Noise. *Electrochem. commun.* **2004**, *6* (11), 1185–1191. https://doi.org/10.1016/j.elecom.2004.09.017.

(37) Bautista, A.; Huet, F. Noise Resistance Applied to Corrosion Measurements IV. Asymmetric Coated Electrodes. *J. Electrochem. Soc.* **1999**, *146* (5), 1730–1736.

(38) Cottis, R. A.; Turgoose, S.; Mendoza-Flores, J. The Effects of Solution Resistance on Electrochemical Noise Resistance Measurements: A Theoretical Analysis. In *Electrochemical noise measurement for corrosion applications, ASTM STP 1277*; Kearns, J. R., Scully, J. R., Roberge, P. R., Reichert, D. L., Dawson, J. L., Eds.; American socienty for testing and materials, 1996; pp 93–100.

(39) Cottis, R. A. Interpretation of Electrochemical Noise Data. *corrosion* **2001**, *57* (3), 265–285.

(40) Pistorius, P. C. Design Aspects of Electrochemical Noise Measurements for Uncoated Metals: Electrode Size and Sampling Rate. *Corros.* **1997**, *53* (4), 273–283. https://doi.org/10.5006/1.3280468.

(41) Kasuya, M.; Sogawa, T.; Masuda, T.; Kamijo, T.; Uosaki, K.; Kurihara, K. Anion Adsorption on Gold Electrodes Studied by Electrochemical Surface Forces Measurement. *J. Phys. Chem. C* **2016**, *120* (29), 15986–15992. https://doi.org/10.1021/acs.jpcc.5b12683.

(42) Lei, H. W.; Uchida, H.; Watanabe, M. Electrochemical Quartz Crystal Microbalance Study of Halide Adsorption and Concomitant Change of Surface Excess of Water on Highly Ordered Au(111). *Langmuir* **1997**, *13* (13), 3523–3528. https://doi.org/10.1021/la960817z.

(43) Shatla, A. S.; Landstorfer, M.; Baltruschat, H. On the Differential Capacitance and Potential of Zero Charge of Au(111) in Some Aprotic Solvents. *ChemElectroChem* **2021**, *8* (10), 1817–1835. https://doi.org/10.1002/celc.202100316.

(44) Lust, E. Zero Charge Potentials and Electrical Double Layer at Solid Electrodes. In *Encyclopedia of Interfacial Chemistry: Surface Science and Electrochemistry*; 2018; pp 316–344. https://doi.org/10.1016/B978-0-12-409547-2.13613-3.

(45) Darowicki, K.; Zielin, A. Joint Time – Frequency Analysis of Electrochemical Noise. *J. Electroanal. Chem.* **2001**, *504*, 201–207.

(46) Gao, R.; Edwards, M. A.; Harris, J. M.; White, H. S. Shot Noise Sets the Limit of Quantification in Electrochemical Measurements. *Curr. Opin. Electrochem.* **2020**, *22*, 170–177. https://doi.org/10.1016/j.coelec.2020.05.010.

(47) Rocha, P. R. F.; Schlett, P.; Kintzel, U.; Mailänder, V.; Vandamme, L. K. J.; Zeck, G.; Gomes, H. L.; Biscarini, F.; De Leeuw, D. M. Electrochemical Noise and Impedance of Au Electrode/Electrolyte Interfaces Enabling Extracellular Detection of Glioma Cell Populations. *Sci. Rep.* **2016**, *6* (September), 1–10. https://doi.org/10.1038/srep34843.

(48) Moulton, S. E.; Barisci, J. N.; Bath, A.; Stella, R.; Wallace, G. G. Studies of Double Layer Capacitance and Electron Transfer at a Gold Electrode Exposed to Protein Solutions. *Electrochim. Acta* **2004**, *49* (24), 4223–4230. https://doi.org/10.1016/j.electacta.2004.03.034.

(49) Adamczyk, Z.; Pomorska, A.; Nattich-Rak, M.; Wytrwal-Sarna, M.; Bernasik, A. Protein Adsorption Mechanisms at Rough Surfaces: Serum Albumin at a Gold Substrate. *J. Colloid*

Interface Sci. **2018**, *530*, 631–641. https://doi.org/10.1016/j.jcis.2018.06.063.

(50) Ying, P.; Viana, A. S.; Abrantes, L. M.; Jin, G. Adsorption of Human Serum Albumin onto Gold: A Combined Electrochemical and Ellipsometric Study. *J. Colloid Interface Sci.* **2004**, *279* (1), 95–99. https://doi.org/10.1016/j.jcis.2004.06.048.